Journal of Alloys and Compounds 828 (2020) 154337

Contents lists available at ScienceDirect

Journal of Alloys and Compounds

journal homepage: http://www.elsevier.com/locate/jalcom

High-responsivity $(In_{0.26}Ga_{0.74})_2O_3$ UV detectors on sapphire realized by microwave irradiation-assisted deposition

Usman Ul Muazzam [a, *], M. Srinidhi Raghavan [a, b], Anamika Singh Pratiyush [a], R. Muralidharan [a], Srinivasan Raghavan [a], Digbijoy N. Nath [a], S.A. Shivashankar [a, **]

[a] Centre for Nano Science and Engineering (CeNSE), Indian Institute of Science (IISc), Bengaluru, 560012, India
[b] BMS College of Engineering, Bengaluru, 560019, India

ARTICLE INFO

Article history:
Received 5 November 2019
Received in revised form
27 January 2020
Accepted 12 February 2020
Available online 21 February 2020

Keywords:
InGaO
MSM photodetector
Microwave-assisted deposition
Tauc's plot

ABSTRACT

We report on the demonstration of $(In_xGa_{1-x})_2O_3$ (InGaO)-based UV photodetectors realized using a low temperature (~200 °C) microwave irradiation-assisted deposition technique. By irradiating a solution of the substituted acetylacetonate (acac) complex, namely $In_{0.6}Ga_{0.4}(acac)_3$, employed as the "single-source precursor", InGaO film was deposited on sapphire substrate, and found to be poly(nano)crystalline, with root mean square (r.m.s). roughness of 8.9 nm. However, the indium content of the film (0.26 mol fraction) was considerably less than in the metal complex (0.6 mol fraction). The optical band gap of the film was found to be 4.5 eV from Tauc's plot, indicative of a low indium mole fraction. This was confirmed using X-ray photoelectron spectroscopy measurements, from which the indium mole fraction was found to be 0.26. Further, the nature of band gap was determined and defect analysis was carried out using, respectively, Tauc's plot and cathodoluminescence (CL) measurements. A planar, interdigitated metal-semiconductor-metal (MSM) photodetector fabricated with the InGaO film exhibited a high responsivity of 16.9 A/W at a bias of 20 V, corresponding to a band edge at ~ 276 nm, with a high photo-to-dark current ratio of ~10^5.

1. Introduction

Wide band gap (WBG) semiconducting oxides such as MgO [1], ZnO [2], In_2O_3 [3], and SnO_2 [4] have drawn the attention of researchers of late due to their properties being conducive to photodetector applications. Recently, Ga_2O_3 has been studied extensively for power electronic devices [5], photodetector applications [6], gas sensing [7], transparent conductive oxide [6], etc. owing to its large bandgap, high critical electric field, and excellent chemical and thermal stability. Ultraviolet photodetectors have (UV-PD) potential applications in flame detection, early missile warning, and biological sensing [8–10]. UV PDs have been realized using various WBG materials like GaN [11], In_2O_3 [12], ZnO [13], Ga_2O_3 [14]. Depending on the application regime, a particular material system is opted for. Although Ga_2O_3 detectors are widely reported [15–17], alloys of the same, particularly InGaO, would enable tuning of the band edge, and hence would be particularly attractive for applications that require UV detection at different wavelengths. Such alloys would also offer possibilities of realizing heterojunctions between InGaO/GaO, and between dissimilar compositions of InGaO, for designing versatile opto-electronic devices.

Whereas InGaO is reported to have been deposited or grown using techniques like molecular beam epitaxy (MBE) [18], mist-chemical vapour deposition (mist-CVD) [19], sol-gel [20], metal-organic vapour phase epitaxy (MOVPE) [21], pulsed laser deposition (PLD) [22,23] and radio frequency (RF) sputtering [24], we report here on the deposition of $In_{0.26}Ga_{0.74}O$ using microwave irradiation-assisted solution-based, low temperature process ($T < 200$ °C) that involves relatively safe precursors and requires a shorter run time. We have employed a single-source precursor, namely, a substituted metal complex, for depositing the film of the substituted metal oxide, InGaO.

2. Experimental section

InGaO films were deposited from a solution, in ethanol and 1-

* Corresponding author.
** Corresponding author.
E-mail addresses: usmaanm@iisc.ac.in (U.U. Muazzam), shivu@iisc.ac.in (S.A. Shivashankar).

https://doi.org/10.1016/j.jallcom.2020.154337
0925-8388/

decanol, of the substituted acetylacetonate complex, $In_xGa_{1-x}(acac)_3$, where x = 0.6. The substituted complex with x = 0.6 was prepared using the metal nitrates, following the procedure detailed in the supplementary information. All chemical reagents used were of analytical-grade purity. To deposit the desired oxide film, a solvent mixture was first prepared using ethanol and 1-decanol in the ratio of 3:5; then 1 mmol of InGa(acac) was added to it, after which the mixture was stirred for 2 h to ensure the complete dissolution of InGa(acac) in the solvent mixture. The substrate used for film deposition was a 1 cm^2 piece of c-plane sapphire. With the substrate immersed in it, the prepared solution was irradiated with microwaves at a power of 300 W for 10 min (Focused microwave reactor, Discover Model, CEM Corp., USA). It was found (by inspection) that a film had been deposited on the substrate, which was ultrasonicated in ethanol for 15 s to remove debris.

3. Results and discussion

3.1. Material properties

The resulting film was characterized by X-ray diffraction (XRD, Rigaku SmartLab, Cu−K_α radiation). The diffraction pattern obtained (Fig. 1) shows broad peaks at 2θ value of 34°, 74° and 76°, making them close to the peaks of γ-Ga_2O_3 reported in previous studies [25]. Furthermore, the average crystallite size was estimated using the Scherrer equation assuming spherical crystallites:

$$D = \frac{K\lambda}{\beta cos(\theta)} \quad (1)$$

where D is crystallite size, $K = 0.94$ (for cubic symmetry), and β is the peak width. Using the β for the (311) reflection at $2\theta = 34°$, the crystallite size is estimated to be ~2.8 nm for the polycrystalline film. Thus, the film is very fine-grained, as evident from the weak and noisy XRD pattern.

X-ray photoelectron spectroscopy (XPS, AXIS Ultra DLD, Kratos Analytical) measurement of the as-deposited film was carried out. Fig. 2a and b shows the XPS spectrum of $In_{3d5/2}$ and Ga_{3d}, respectively. The peaks at binding energy value of 20.2 eV and 444.4 eV correspond respectively to the Ga−O bond and In−O bonds [26,27]. The stoichiometry of metals in the film was calculated using the relation:

$$\frac{x}{1-x} = \frac{Area_{In3d5/2}}{Area_{Ga3d}} * \frac{RSF_{Ga3d}}{RSF_{In3d5/2}} \quad (2)$$

Here, x is the mole fraction of indium (In) in the film, and RSF is the "relative sensitivity factor". The mole fraction of In was found to be 26.6%, which shows that the film is Ga-rich. In the substituted binary oxide InGaO, the incorporation of indium is difficult because the Ga−O bond is stronger than the In−O bond. That is, Ga etches the In−O bond and forms the Ga−O bond because it is thermodynamically more favourable; by contrast, In does not etch the Ga−O bond [18].

Based on the In−Ga composition of the oxide film deduced from XPS data, the lattice constant of the substituted oxide can be calculated. This is because InGaO has been shown to follow Vegard's law [28] for the relating the lattice constant a of the substituted oxide to its composition. Thus, using data in Refs. [3,29], we have:

$$a_{(InxGa1-x)2O3} = X.\ a_{In2O3} + (1-X).\ a_{Ga2O3} \quad (3)$$

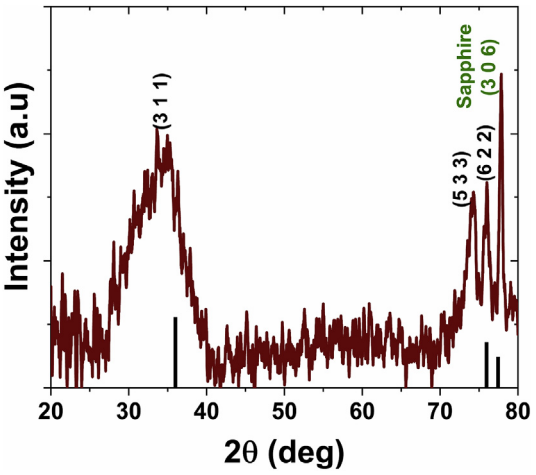

Fig. 1. XRD θ-2θ plot of InGaO. Vertical black lines shows peak position of γ-Ga_2O_3.

$a_{In2O3} = 10.117$Å[3]

$a_{Ga2O3} = 8.238$ Å[29]

From these $a_{(InxGa1-x)2O3}$ is found to be equal to 8.738 Å.

$$d_{hkl} = \frac{a_{(InxGa1-x)2O3}}{\sqrt{h2+k2+l2}} \quad (4)$$

for (3 1 1) reflection we have $d_{311} = 2.634$ Å.

Bragg's angle for (3 1 1) reflection can be found from Bragg's law as

$$2\theta = 2\sin^{-1}\left(\frac{\lambda}{2d311}\right) \quad (5)$$

$= 34.008°$

This is the same as what is obtained experimentally, confirming that the mole fraction of gallium in the film is higher than it is in the precursor compound.

The morphology of the film was examined by field-emission scanning electron microscopy (FE-SEM, GEMINI Ultra 55, Carl Zeiss). The deposited film was smooth with uniform coverage, as shown in Fig. 3a. The energy-dispersive X-ray spectrum (EDS) (Fig. 3b) confirms that the film is Ga-rich. The thickness of the film was determined using cross-sectional SEM and was found to be 104 nm (Fig. 3c). The r.m.s. roughness was measured using atomic force microscopy (Dimension ICON, Bruker) in the tapping mode and found to be 8.9 nm (Fig. 3d).

To determine the band gap of the substituted oxide, Tauc's plot was obtained from the absorption coefficients measured using a UV−Vis−NIR spectrophotometer (UV-3600, Shimadzu). The band gap, deduced by extrapolating the linear region to the energy axis (Fig. 4a), was found to be 4.4 eV, showing a slight deviation from Vegard's law. This deviation could be because of "defect tails" spanning the bandgap [30]. As can be seen from Fig. 4a, there is an exponential onset in the Tauc plot, known as the Urbach tail. An analysis of the Urbach tail was therefore carried out. The span of defect tail can be found by plotting log(α) *vs.* energy, where α is the absorption coefficient; the inverse of the slope of the resulting line gives the "Urbach energy". From inset of Fig. 4a, the Urbach energy is found to be 0.47 eV. To deduce the nature of the bandgap in the substituted oxide, Tauc's relation was plotted on the log scale:

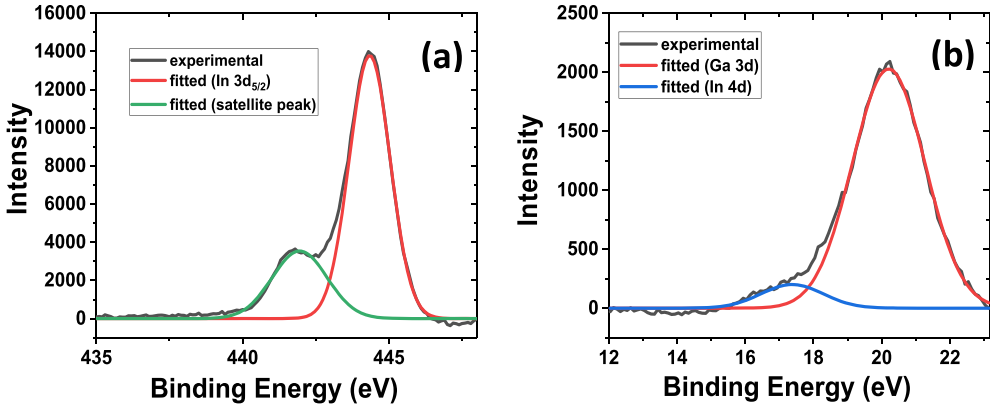

Fig. 2. XPS fitting for (a) In $3d_{5/2}$ spectrum of InGaO (b) Ga 3d core level spectrum.

$$\log(\alpha h\nu) = \log(B) + n\log(h\nu - E_G) \quad (6)$$

where n is the slope of the curve and log(B) is a constant. The slope was found to be 0.55, which implies the band gap in InGaO (of the present composition) is direct (Fig. 4b).

3.2. Device properties

To characterize InGaO optically, an MSM PD was fabricated using the deposited film, with an interdigitated electrode geometry obtained from the i-line lithography process. The device comprises 36 interdigitated fingers, with finger width of 4 μm and finger spacing 6 μm, resulting in an effective detector area of 260 × 300 μm^2. The schematic of the MSM PD is shown in Fig. 5a, with Fig. 5b showing an optical micrograph of the same.

Spectral responsivity (SR) of the fabricated MSM PD was measured using a quantum efficiency setup, the details of which are reported elsewhere [31]. The SR spectra show a band-edge at 275.5 nm, which matches well with the UV–Vis measurement. Fig. 5c shows the variation of SR with wavelength at different voltages, on the linear scale (5 V, 10 V, 15 V and 20 V), whereas Fig. 5d shows the variation on the semilog scale. The peak SR is at 275.5 nm. The UV-to-visible rejection ratio (UV–Vis RR) was calculated by dividing the SR value at 275.5 nm by the SR value at 400 nm. The UV–Vis RR observed at 5 V was found to be ~10^3. The peak SR value of 16.9 A/W is measured at a bias of 20 V.

There are two kinks in the spectral response plot - one at 289 nm and the other at around 329 nm. To investigate the origin of

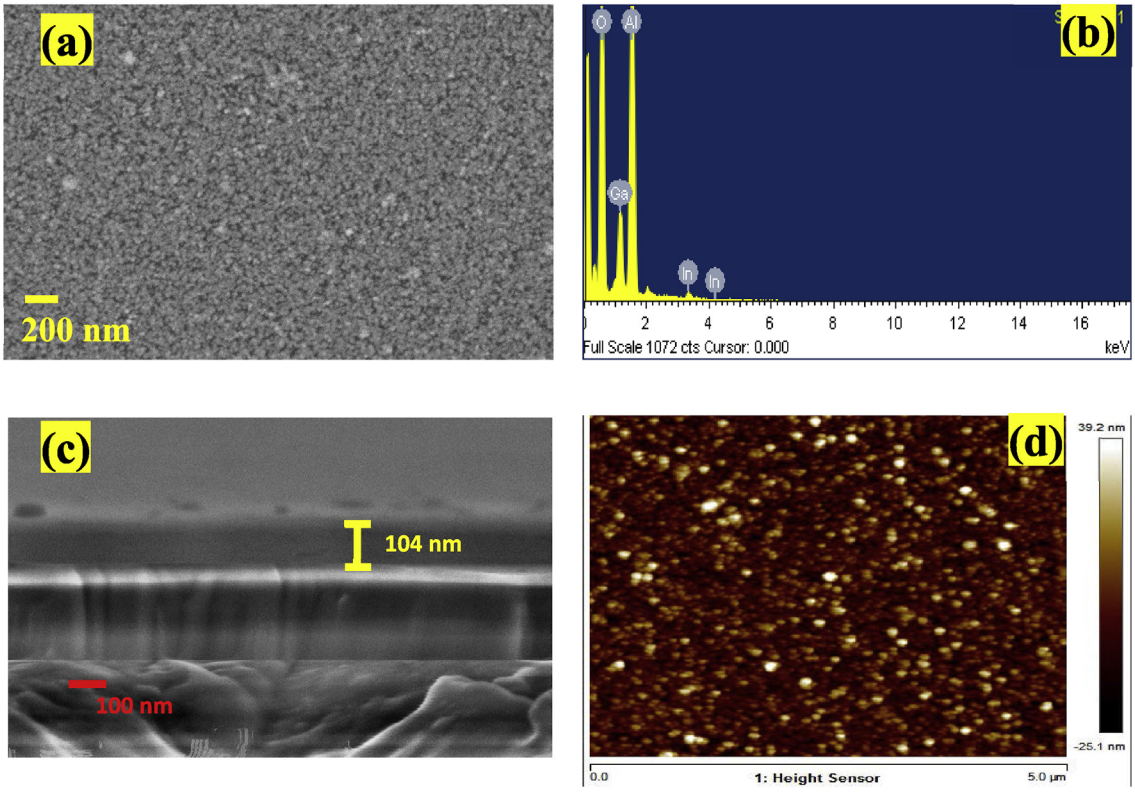

Fig. 3. (a) SEM micrograph of the as-deposited polycrystalline InGaO film (b) EDS spectrum showing a Ga-rich film (c) cross-sectional SEM image gives thickness of 104 nm (d) R.M.S roughness of film is 8.9 nm.

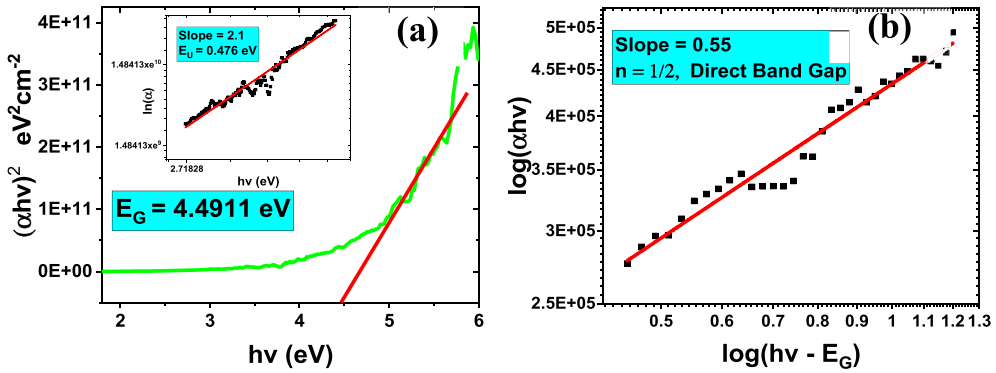

Fig. 4. (a) Extracted bandgap from Tauc's plot is 4.5 eV, Inset shows variation of absorption coefficient with incident photon energy in semilog scale gives Eu = 0.47 eV (b) Tauc's relation plotted in log-log scale reveals that the bandgap is direct.

the kinks, cathodoluminescence (CL) spectra were obtained. The CL spectra exhibit peaks at 326 nm, 398 nm, 554 nm, and 650 nm measured at a gun voltage of 10 keV (Fig. 5e). The peak at 326 nm is due to self-trapped holes [19]. The kink at 289 nm vanishes as applied voltage increases; this can be attributed to dissociation of excitons. which can exist in oxide semiconductors even at room temperature because of the large Fröhlich coupling coefficient attributable to the highly polar metal-oxygen bond [32,33].

Fig. 6a shows the current-voltage (I–V) characteristic of the MSM PD. The measured dark current was found to be 200 pA at a bias of 20 V, increasing to 35 μA upon illumination with 276 nm wavelength, at a bias of 20 V. Thus, under UV illumination, the current increases by five orders of magnitude. This ratio of photo-to-dark current (PDR) gives information about the signal-to-noise

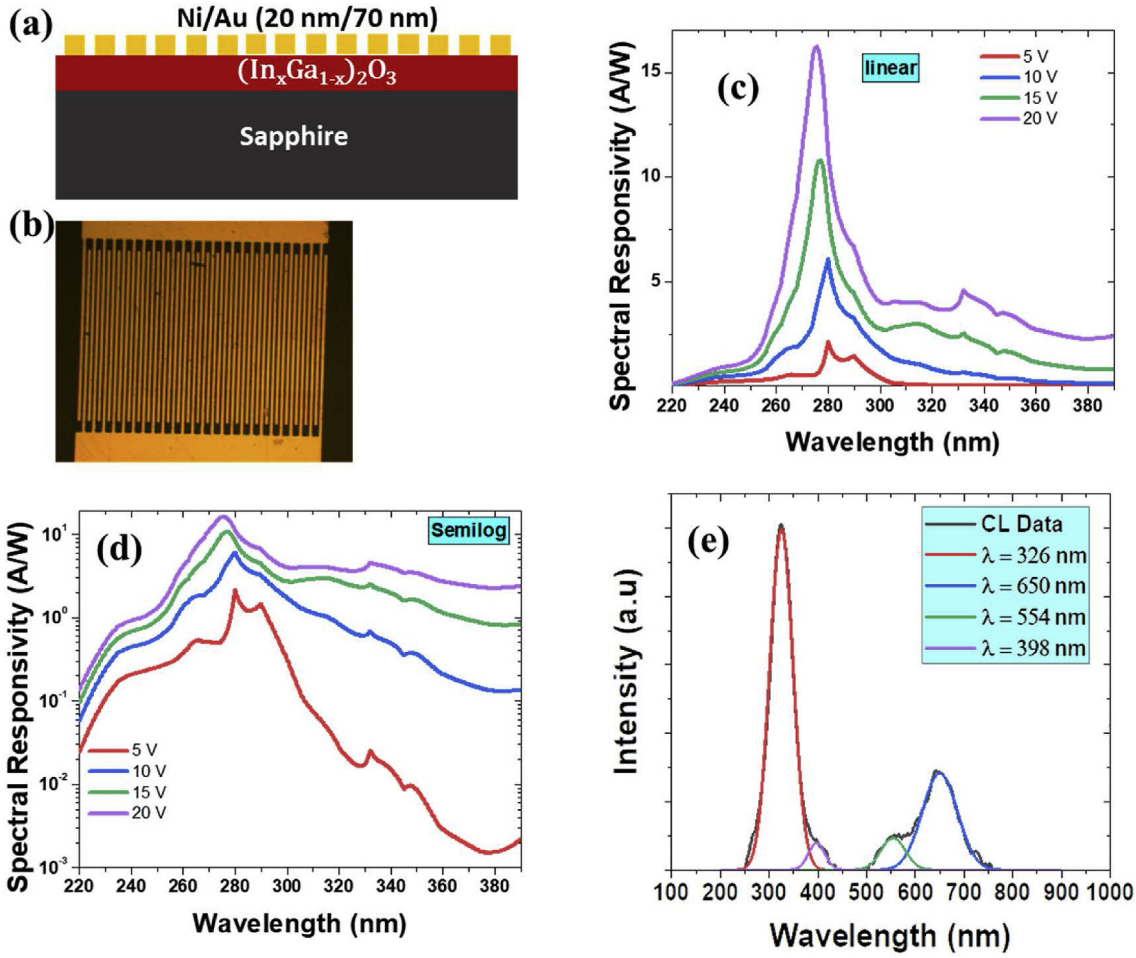

Fig. 5. (a) Schematic of MSM PD on InGaO (side view) (b) Shows optical micrograph of MSM PD on InGaO (top view) (c) Shows variation of spectral response with wavelength as a function of voltage in linear scale (d) variation of spectral response with wavelength as a function of voltage in log scale. Also can be seen that the UV–Visible rejection ratio is ~10^3 at 5 V (e) CL spectra of InGaO measured at 10 keV gun voltage.

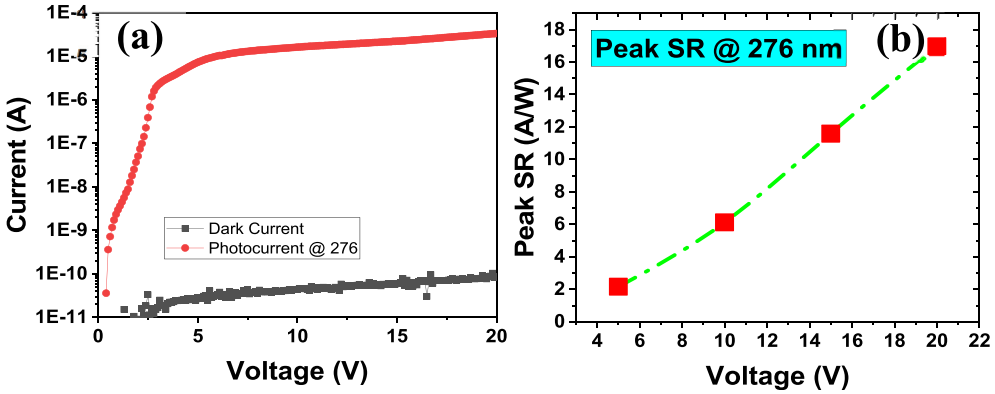

Fig. 6. (a) Variation of photocurrent (at 276 nm) and dark current with applied voltage (b) Variation of peak SR (at 276 nm) with applied voltage.

Table 1

S·NO	Deposition method	**Peak SR (A/W)**	PDR	UV–Vis RR	Reference
1	PLD	0.5	–	10^3	[38]
2	Sputtering	6.9×10^{-5}	10^2	1.5×10^4	[24]
3	PLD	6.12	10^2	–	[23]
4	Sol-gel	0.4	–	–	[20]
5	PLD	30	–	–	[22]
6	Microwave irradiation	16.9	10^5	10^3	This work

ratio, which is determined by the following formula:

$$\mathrm{PDR} = \frac{I_{Photo} - I_{Dark}}{I_{Dark}} \tag{7}$$

where I_{Photo} is the photocurrent and I_{Dark} is the dark current.

Fig. 6b shows the variation of the peak SR with the applied voltage under illumination at 276 nm. The peak SR was found to increase with increasing applied voltage. The peak SR at 20 V is 16.9 A/W, which is much larger than the theoretical SR calculated assuming 100% external quantum efficiency (η). The theoretical SR of a photodetector can be calculated using the following expression:

$$\mathrm{R_{Th}} = \frac{q\eta}{h\upsilon} \tag{8}$$

where q is the electronic charge and hυ is the photon quantum energy.

The measured responsivity is determined using the following relation:

$$\mathrm{R} = \frac{I_{Photo} - I_{Dark}}{P_{Optical}} \tag{9}$$

where $P_{Optical}$ is the optical power employed.

The theoretical SR value at 275.5 nm comes out to be 222.17 mA/W. This value is much less than the peak SR measured at 275.5 nm, implying that there is gain in the device [34–36]. This gain may be attributed to photo-induced barrier lowering. Metal oxides are notorious for strong hole-phonon coupling (self-trapped hole) [37], which makes the mobility of holes much lower than that of electrons. This leads to transit time gain in the device additionally when UV light falls on the device; that is, due to band bending in the depletion region, holes move towards the semiconductor-metal interface, which has lots of trap states in the forbidden gap. These holes get trapped there, making the interface region positively charged. To maintain charge neutrality, band bending decreases, because of reduction in depletion charge. This leads to a reduction in barrier height, known as photoinduced barrier lowering [36]. Table 1 lists the properties of the photodetectors fabricated by different groups in the InGaO material system.

4. Conclusions

In conclusion, we have reported microwave irradiation-assisted deposition of $(In_xGa_{1-x})_2O_3$ on c-plane sapphire substrate, employing a substituted metal complex as the "single-source precursor" to the substituted oxide. The deposited film was found to be poly(nano)crystalline with a Ga-rich composition, and was characterized by XRD, XPS, CL, SEM, AFM and UV–Visible spectroscopy. A solar-blind UV photodetector with good spectral response was demonstrated on the $(In_xGa_{1-x})_2O_3$ deposited on sapphire substrate.

Funding

This work was supported in part by the Space Technology Cell (STC) and in part by the Department of Science and Technology (DST) through the Water Technology Initiative (WTI). The authors also acknowledge funding from MHRD, MeitY and DST Nano Mission for supporting the facilities at Centre for Nano Science and Engineering (CeNSE). This work was also partially funded by US AFOSR, USAF grant number FA2386-19-1-4026, Program manager: Ali Sayir.

Declaration of competing interest

The authors declare that they have no competing interests.

CRediT authorship contribution statement

Usman Ul Muazzam: Conceptualization, Methodology, Validation, Formal analysis, Investigation, Software, Data curation, Visualization, Writing - original draft. **M. Srinidhi Raghavan:** Validation, Formal analysis, Investigation, Data curation, Visualization. **Anamika Singh Pratiyush:** Formal analysis, Visualization. **R. Muralidharan:** Validation, Resources, Supervision, Visualization, Writing - review & editing, Funding acquisition. **Srinivasan Raghavan:** Validation, Resources, Supervision, Visualization, Writing - review & editing, Funding acquisition. **Digbijoy N. Nath:** Validation, Resources, Supervision, Visualization, Writing - review & editing, Funding acquisition. **S.A. Shivashankar:** Conceptualization, Project administration, Validation, Resources, Supervision, Visualization, Writing - review & editing, Funding acquisition.

Acknowledgements

The authors would like to acknowledge the staff of Micro Nano Characterization Facility (MNCF) and National Nano Fabrication Centre (NNFC) at CeNSE, IISc.

Appendix A. Supplementary data

Supplementary data to this article can be found online at https://doi.org/10.1016/j.jallcom.2020.154337.

References

[1] R.A. Ismail, K.S. Khashan, M.F. Jawad, A.M. Mousa, F. Mahdi, Preparation of low cost n-ZnO/MgO/p-Si heterojunction photodetector by laser ablation in liquid and spray pyrolysis, Mater. Res. Express 5 (2018), https://doi.org/10.1088/2053-1591/aac24e.

[2] K.M. Gupta, N. Gupta, Recent advances in semiconducting materials and devices 80 (2015) 531–562, https://doi.org/10.1007/978-3-319-19758-6_16.

[3] F. Fuchs, F. Bechstedt, Indium-oxide polymorphs from first principles: quasiparticle electronic states, Phys. Rev. B Condens. Matter 77 (2008) 1–10, https://doi.org/10.1103/PhysRevB.77.155107.

[4] H. Bendjedidi, A. Attaf, H. Saidi, M.S. Aida, S. Semmari, A. Bouhdjar, Y. Benkhetta, Properties of n-Type SnO2 semiconductor prepared by spray ultrasonic technique for photovoltaic applications, J. Semiconduct. 36 (2015), https://doi.org/10.1088/1674-4926/36/12/123002, 0–4.

[5] M. Higashiwaki, A. Kuramata, H. Murakami, Y. Kumagai, State-of-the-art technologies of gallium oxide power devices, J. Phys. D Appl. Phys. 50 (2017) 333002, https://doi.org/10.1088/1361-6463/aa7aff.

[6] M. Orita, H. Ohta, M. Hirano, H. Hosono, Deep-ultraviolet transparent conductive ß-Ga_2O_3 thin films, Appl. Phys. Lett. 77 (2000) 4166–4168, https://doi.org/10.1063/1.1330559.

[7] M. Isai, T. Yamamoto, T. Torii, Preparation and Evaluation of Ga_2O_3 Oxygen Sensors, vol. 36, 2012, 2012, https://www.jstage.jst.go.jp/article/tmrsj/35/4/35_897/_pdf.

[8] E. Monroy, E. Muñoz, F.J. Sánchez, F. Calle, E. Calleja, B. Beaumont, P. Gibart, J.A. Muñoz, F. Cussó, High-performance GaN p-n junction photodetectors for solar ultraviolet applications, Semicond. Sci. Technol. 13 (1998) 1042–1046, https://doi.org/10.1088/0268-1242/13/9/013.

[9] E. Monroy, F. Omnès, F. Calle, Wide-bandgap semiconductor ultraviolet photodetectors, Semicond. Sci. Technol. 18 (2003), https://doi.org/10.1088/0268-1242/18/4/201.

[10] H. Chen, K. Liu, L. Hu, A.A. Al-Ghamdi, X. Fang, New concept ultraviolet photodetectors, Mater. Today 18 (2015) 493–502, https://doi.org/10.1016/j.mattod.2015.06.001.

[11] M.L. Lee, J.K. Sheu, W.C. Lai, S.J. Chang, Y.K. Su, M.G. Chen, C.J. Kao, G.C. Chi, J.M. Tsai, GaN Schottky barrier photodetectors with a low-temperature GaN cap layer, Appl. Phys. Lett. 82 (2003) 2913–2915, https://doi.org/10.1063/1.1570519.

[12] S. Rajamani, K. Arora, A. Konakov, A. Belov, D. Korolev, A. Nikolskaya, A. Mikhaylov, S. Surodin, R. Kryukov, D. Nikolitchev, A. Sushkov, D. Pavlov, D. Tetelbaum, M. Kumar, M. Kumar, Deep UV narrow-band photodetector based on ion beam synthesized indium oxide quantum dots in Al_2O_3 matrix, Nanotechnology 29 (2018), https://doi.org/10.1088/1361-6528/aabfaf.

[13] S. Liang, H. Sheng, Y. Liu, Z. Huo, Y. Lu, H. Shen, ZnO Schottky ultraviolet photodetectors, J. Cryst. Growth 225 (2001) 110–113, https://doi.org/10.1016/S0022-0248(01)00830-2.

[14] A. Singh Pratiyush, U. Ul Muazzam, S. Kumar, P. Vijayakumar, S. Ganesamoorthy, N. Subramanian, R. Muralidharan, D.N. Nath, Optical Float-Zone Grown Bulk β-Ga_2O_3-based Linear MSM Array of UV-C Photodetectors, IEEE Photonics Technol. Lett, 2019, pp. 923–926.

[15] S. Oh, C.K. Kim, J. Kim, High responsivity β-Ga_2O_3 metal-semiconductor-metal solar-blind photodetectors with ultraviolet transparent graphene electrodes, ACS Photonics 5 (2018) 1123–1128, https://doi.org/10.1021/acsphotonics.7b01486.

[16] M. Ai, D. Guo, Y. Qu, W. Cui, Z. Wu, P. Li, L. Li, W. Tang, Fast-response solar-blind ultraviolet photodetector with a graphene/β-Ga_2O_3/graphene hybrid structure, J. Alloys Compd. 692 (2017) 634–638, https://doi.org/10.1016/j.jallcom.2016.09.087.

[17] A. Singh Pratiyush, S. Krishnamoorthy, S. Vishnu Solanke, Z. Xia, R. Muralidharan, S. Rajan, D.N. Nath, High responsivity in molecular beam epitaxy grown β-Ga_2O_3 metal semiconductor metal solar blind deep-UV photodetector, Appl. Phys. Lett. 110 (2017) 1–6, https://doi.org/10.1063/1.4984904.

[18] P. Vogt, O. Bierwagen, Kinetics versus thermodynamics of the metal incorporation in molecular beam epitaxy of $(In_xGa_{1-x})_2O_3$, Apl. Mater. 4 (2016), https://doi.org/10.1063/1.4961513.

[19] N. Suzuki, K. Kaneko, S. Fujita, Growth of corundum-structured $(In_xGa_{1-x})_2O_3$ alloy thin films on sapphire substrates with buffer layers, J. Cryst. Growth 401 (2014) 670–672, https://doi.org/10.1016/j.jcrysgro.2014.02.051.

[20] Y. Kokubun, T. Abe, S. Nakagomi, Sol-gel prepared $(Ga_{1-x}In_x)_2O_3$ thin films for solar-blind ultraviolet photodetectors, Phys. Status Solidi Appl. Mater. Sci. 207 (2010) 1741–1745, https://doi.org/10.1002/pssa.200983712.

[21] M. Baldini, M. Albrecht, D. Gogova, R. Schewski, G. Wagner, Effect of indium as a surfactant in (Ga1-xInx)2O3 epitaxial growth on β-Ga_2O_3 by metal organic vapour phase epitaxy, Semicond. Sci. Technol. 30 (2015), https://doi.org/10.1088/0268-1242/30/2/024013.

[22] F. Zhang, H. Li, M. Arita, Q. Guo, Ultraviolet detectors based on $(GaIn)_2O_3$ films, Opt. Mater. Express 7 (2017) 3769, https://doi.org/10.1364/ome.7.003769.

[23] K. Zhang, Q. Feng, L. Huang, Z. Hu, Z. Feng, A. Li, H. Zhou, X. Lu, C. Zhang, J. Zhang, Y. Hao, $(In_xGa_{1-x})_2O_3$ photodetectors fabricated on sapphire at different temperatures by PLD, IEEE Photonics J. 10 (2018), https://doi.org/10.1109/JPHOT.2018.2841968.

[24] T.-H. Chang, S.-J. Chang, I.E.E.E. Fellow, W.-Y. Weng, C.-J. Chiu, C.-Y. Wei, Amorphous indium – gallium – oxide, IEEE Photon. Technol. Lett. 27 (2015) 2083–2086, https://doi.org/10.1109/LPT.2015.2453317.

[25] O. Nikulina, D. Yatsenko, O. Bulavchenko, G. Zenkovets, S. Tsybulya, Debye function analysis of nanocrystalline gallium oxide γ-Ga_2O_3, Zeitschrift Fur Krist. - Cryst. Mater. 231 (2016) 261–266, https://doi.org/10.1515/zkri-2015-1895.

[26] C. Huang, W. Mu, H. Zhou, Y. Zhu, X. Xu, Z. Jia, L. Zheng, X. Tao, Effect of OH - on chemical mechanical polishing of β-Ga_2O_3 (100) substrate using an alkaline slurry, RSC Adv. 8 (2018) 6544–6550, https://doi.org/10.1039/c7ra11570a.

[27] M. Himmerlich, Surface Characterization of Indium Compounds as Functional Layers for (Opto) Electronic and Sensoric Applications, Technische Universität Ilmenau, 2008.

[28] H. Peelaers, D. Steiauf, J.B. Varley, A. Janotti, C.G. Van De Walle, $(In_xGa_{1-x})_2O_3$ alloys for transparent electronics, Phys. Rev. B Condens. Matter 92 (2015) 1–6, https://doi.org/10.1103/PhysRevB.92.085206.

[29] M. Zinkevich, F.M. Morales, H. Nitsche, M. Ahrens, M. Rühle, F. Aldinger, Microstructural and thermodynamic study of γ-Ga_2O_3, Zeitschrift Fuer Met. Res. Adv. Tech. 95 (2004) 5–11, https://doi.org/10.3139/146.018018.

[30] A.S. Hassanien, A.A. Akl, Influence of composition on optical and dispersion parameters of thermally evaporated non-crystalline $Cd_{50}S_{50-x}Se_x$ thin films, J. Alloys Compd. 648 (2015) 280–290, https://doi.org/10.1016/j.jallcom.2015.06.231.

[31] P. Jaiswal, U. Ul Muazzam, A.S. Pratiyush, N. Mohan, S. Raghavan, R. Muralidharan, S.A. Shivashankar, D.N. Nath, Microwave irradiation-assisted deposition of Ga_2O_3 on III-nitrides for deep-UV opto-electronics, Appl. Phys. Lett. 112 (2018), https://doi.org/10.1063/1.5010683.

[32] T. Kazimierczuk, D. Fröhlich, S. Scheel, H. Stolz, M. Bayer, Giant Rydberg excitons in the copper oxide Cu_2O, Nature 514 (2014) 343–347, https://doi.org/10.1038/nature13832.

[33] A. Segura, L. Artús, R. Cuscó, R. Goldhahn, M. Feneberg, Band gap of corundumlike α-Ga_2O_3 determined by absorption and ellipsometry, Phys. Rev. Mater. 1 (2017), 024604, https://doi.org/10.1103/PhysRevMaterials.1.024604.

[34] S. Rathkanthiwar, A. Kalra, S.V. Solanke, N. Mohta, R. Muralidharan, S. Raghavan, D.N. Nath, Gain mechanism and carrier transport in high responsivity AlGaN-based solar blind metal semiconductor metal photodetectors, J. Appl. Phys. 121 (2017), https://doi.org/10.1063/1.4982354, 0–10.

[35] A.M. Armstrong, M.H. Crawford, A. Jayawardena, A. Ahyi, S. Dhar, Role of self-trapped holes in the photoconductive gain of β -gallium oxide Schottky diodes, J. Appl. Phys. 119 (2016) 1–7, https://doi.org/10.1063/1.4943261.

[36] O. Katz, V. Garber, B. Meyler, G. Bahir, J. Salzman, Gain mechanism in GaN Schottky ultraviolet detectors, Appl. Phys. Lett. 79 (2001) 1417–1419, https://doi.org/10.1063/1.1394717.

[37] J.B. Varley, A. Janotti, C. Franchini, C.G. Van De Walle, Role of self-trapping in luminescence and p-type conductivity of wide-band-gap oxides, Phys. Rev. B Condens. Matter 85 (2012) 2–5, https://doi.org/10.1103/PhysRevB.85.081109.

[38] Z. Zhang, H. Von Wenckstern, J. Lenzner, M. Lorenz, M. Grundmann, Visible-blind and solar-blind ultraviolet photodiodes based on $(In_xGa_{1-x})_2O_3$, Appl. Phys. Lett. 108 (2016), https://doi.org/10.1063/1.4944860.